Magazine of Civil Engineering

journal homepage: http://engstroy.spbstu.ru/

ISSN 2712-8172

Research article

UDC 693.22

DOI: 10.34910/MCE.128.5

Numerical prediction of crack formation in historic masonry buildings

G.A. Iovlev ✉, ***N.V. Belov, A.G. Zileev***

Saint-Petersburg Mining University, St. Petersburg, Russian Federation
✉ *gregoriiovlev@gmail.com*

Keywords: constitutive modelling, masonry, brick, compression testing, numerical methods, PLAXIS, mortar, cracks

Abstract. This article investigated mechanical behavior of the masonry of historic buildings. It was assumed that reliable cracking processes can be obtained by modeling masonry as a continuous medium and using the Jointed Masonry Model (JMM). The paper gives an analytical review of JMM, identifying the input parameters required for its use. Laboratory tests of brick blocks and mortar for uniaxial compression were carried out and the results of these tests are presented. It is proposed to use the triaxial compression test methodology for rocks for cylindrical samples drilled from bricks. Based on the obtained laboratory data, a method for obtaining input parameters for JMM was proposed. To verify the obtained input parameters of JMM, the construction of a numerical model to predict the stress-strain state of historic masonry buildings was proposed. As an example, old workshop buildings located in the area near St. Petersburg were considered. The results of numerical calculations were compared with the results of building facades surveys for the presence of cracks and opening widths in them. It was found that the zones of the greatest shear deformations were formed mainly in the corners of window and door openings, mainly in the right and left parts of the model. Their position had a qualitative convergence with the results of surveys. The process of formation and qualitative change of zones of limiting compressive and tensile stresses that were formed in the walls of buildings was analyzed using different sets of input parameters of JMM. The influence of dilatancy effects on the stress-strain state was also considered. The study found that a reliable description of the mechanical condition of historic masonry can be obtained using JMM, whose input parameters should be based on the results of laboratory tests. The conducted work showed that along with classical methods of surveys it was possible to use methods of numerical modeling to predict areas where crack propagation occur for historic masonry buildings.

Citation: Iovlev, G.A., Belov, N.V., Zileev, A.G. Numerical prediction of crack formation in historical masonry buildings. Magazine of Civil Engineering. 2024. 17(4). Article no. 12805. DOI: 10.34910/MCE.128.5

1. Introduction

Nowadays the preservation of old historic buildings is an important task in the construction industry. Historic centers of modern cities are formed mainly by old brick buildings. In the conditions of rapid urban development, many new buildings and underground structures are being constructed in close proximity to historic buildings. It becomes relevant to assess the current state of historic buildings and the possibility of their reconstruction for further exploitation. The question arises about the ways to predict the fracturing accumulated in brick buildings during their existence.

Over many years of existence, accumulated deformations in foundation stone structures lead to emergence of cracks, brick falling out, and peeling of plaster. These are characteristic features of many historic buildings, because engineering methods of designing foundations at that time could not accurately predict the geomechanical processes occurring in the surrounding soils.

The object of the study is the masonry of historic buildings. The aim of the study is to obtain a reliable prediction of crack development in historic brick buildings. In the framework of continuum mechanics and solid mechanics approaches, when implemented by numerical methods, more sophisticated and complex constitutive models become one of the main ways to increase the reliability of the description of the mechanical state.

Researchers have developed a large number of nonlinear constitutive models aimed at determining the tensile strength of masonry and bricks [1, 2], which consider the anisotropy of properties caused by mortar joints [3, 4] and complex interaction between the masonry blocks [5–10]. However, most of these approaches are implemented under plane stress or plane strain conditions, which leads to negligible effects on the macroscopic elastic behavior [11], but significantly affects the nonlinear response [12]. More complex three-dimensional models have been proposed within the continuum [13] and discrete [14–16] approaches, for example, models that take into account the accumulation of material fracture provide a good representation of the post-fracture behavior [17, 18]. Only some of them consider the nonlinear behavior of both the soil mass and crack development phenomena in masonry for the two-dimensional [19–21] and three-dimensional [22–26] cases.

Italian researchers [27, 28] proposed a three-dimensional nonlinear model for the mechanical behavior of brick structures called Jointed Masonry Model (JMM). JMM is a modification of the better known Jointed Rock Model (JRM) [29, 30]. In the same studies, on verification tests, it is shown that JMM is able to reliably reproduce various mechanical tests of brick masonry units. The advantages of numerical modeling are demonstrated in the article [31], and the possibilities of PLAXIS for solving geotechnical problems are given in [32–34].

This study aimed to accurately describe the mechanical condition of historic masonry. However, the masonry of historic buildings is often characterized by heterogeneity of physical and mechanical properties [53]. Work [54] describes the causes of degradation of ceramic bricks and, consequently, justifies the combined effect of the aging process on the strength of the masonry. The presence of holes inside the bricks, caused by the production technology, is the cause of stress redistribution [35]. This factor increases the difficulty and possibility of data systematization from existing researches.

At the same time, when considering historic masonry, large-scale laboratory tests composed of assembled wall sections become difficult to achieve. This means that it is impossible to verify the correct operation of JMM based on these tests.

It can be assumed that for the mechanical behavior of historic brick masonry, the determination of the input parameters of JMM requires a set of mechanical laboratory tests. These tests should be performed separately for bricks and masonry. Taking into account the variety of influencing factors, the input parameters thus obtained will describe the mechanical behavior of a particular object. To verify the obtained parameters, it is possible to compare the crack development pattern in the numerical model with that obtained from the survey results.

Under these conditions, the development of a methodology for obtaining input parameters for JMM of historic masonry buildings with their further verification with the results of surveys becomes an urgent task.

2. Methods

The paper describes the process of deformation and crack formation in historic masonry building structures using a user-defined JMM in the PLAXIS 3D software package.

In order to determine the input parameters of the model, an analytical review of JMM is performed. To determine some of the input parameters for JMM, a set of laboratory tests is performed. For finding the cohesion and internal friction angle of bricks and mortar, either uniaxial tensile (UT) or triaxial tests (TXT) must be performed. Since masonry structures are under volumetric stress conditions, TXT is more preferable.

The tests performed for masonry structures are not enough to specify all parameters for JMM. To determine the remaining parameters, additional lab tests were carried out and data from tests on bricks and mortar from published researches results was used [38–40]. For example, the paper [41] summarizes the information about the deformation parameters of bricks and mortar.

There are also investigations aimed to determine the strength properties of bricks and mortar. In [42–45] results from tests on brick masonry under different types of stress-strain state are presented. A number of works [46–51] investigates the bond strength between mortar and brick as well as the mechanical parameters of masonry mortar. Articles [52–54] provide data on mortar tests in triaxial compression tools. The obtained input parameters are summarized and given in the table below.

It is also necessary to verify the obtained input parameters. For this purpose, a numerical model of the building under consideration is built. The mechanical state of the numerical model is reduced to the mechanical state of the building by loading the building model with the given precipitation accumulated over the period of the building existence[1].

2.1. Constructive Design of the Workshop Building

One building of the 17 forts and batteries erected on the Kronstadt roadstead is considered as an example of historic masonry. The fort was originally built of wood in 1724. After a major flood in 1824, the structures were rebuilt in stone in 1833. There are 12 buildings on the fort's territory. It lost its military significance by the beginning of the 20th century, but it was still used in the defense of Leningrad (St. Petersburg) during the World War II. The right-flank curtain building (workshops) was built in 1914 and is located in the southwestern part of the fort. Fig. 1 shows a general view of the central and inner facades of the building.

Figure 1. General view of the workshops[2].

The workshops are located between the horseshoe shaped tower (on the right in fig. 1) and the half circular tower (on the left in fig. 1). Fig. 2 shows a first-floor plan of the building.

Building foundation is a strip, with a heterogeneous structure, which include different components, such as granite blocks 10–50 cm in height, ceramic bricks and limestone. Lime-sand and cement-sand mortar was used as a binder. The depth of the foundations reaches 6.4 m from the first-floor level.

[1] Forty Kronshtadskoĭ kreposti – shedevry rossiĭskogo inzhenernogo dela pervoĭ poloviny XIX v. [The forts of the Kronstadt Fortress are masterpieces of Russian engineering in the first half of the 19th century]. [Online] URL: https://youtu.be/vjlP8JxezHk?si=W-f2NJ3NrvxOagfw (reference date: 24.06.2024); Yandex Maps [Online]. URL: https://yandex.ru/maps/-/CDGOI-LS (reference date: 24.06.2024).

[2] Forty Kronshtadskoĭ kreposti – shedevry rossiĭskogo inzhenernogo dela pervoĭ poloviny XIX v. [The forts of the Kronstadt Fortress are masterpieces of Russian engineering in the first half of the 19th century]. [Online] URL: https://youtu.be/vjlP8JxezHk?si=W-f2NJ3NrvxOagfw (reference date: 24.06.2024); Yandex Maps [Online]. URL: https://yandex.ru/maps/-/CDGOI-LS (reference date: 24.06.2024).

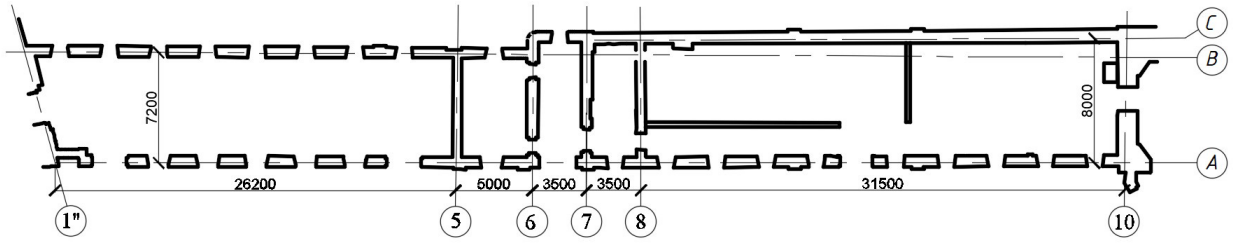

Figure 2. First floor plan of the workshops[3].

The walls are made of ceramic solid bricks using a complex lime-sand mortar. The outer walls are 2.5 bricks thick, with a total width of 640–705 mm. The walls from "C" axis to 10-axis reach at least 850 mm wide. The internal walls in the middle (near the stairwells) are 2.5 bricks thick, with a total width of 600–700 mm.

The ceilings are mainly in the form of concrete arches supported on metal beams. Fig. 3 shows their general view. As a coarse filler for the slabs crushed bricks are used. The average height of the slabs is 25 cm.

Figure 3. General view of the slab structures[4].

2.2. Jointed Masonry Model

2.2.1. Strength parameters of the model

To analyze mechanical behavior of masonry structures, JMM was used [27, 28]. As it was mentioned above, this model is a modification of the better known JRM implemented in PLAXIS 3D. JRM is an anisotropic elastoplastic model designed to simulate the behavior of stratified and fractured rock mass.

JRM assumes that there is rock mass with a definite layering direction and preferential crack orientations. A total of three such orientations can be specified. Each i-th direction has its own normal and shear stresses (Fig. 4). Shear stresses are limited according to Mohr-Coulomb failure criterion. When the maximum shear stress on one of the directions is achieved, plastic flow occurs and both associated and unassociated flow rules can be used.

In addition to the shearing along the crack planes, the tensile stresses are limited by a specified value according to Rankine's criterion. The Mohr-Coulomb yield function and the tensile yield limit are defined by equations (1) and (2):

$$f_i^C = \left|\tau_{s,i}\right| + \sigma_{n,i}\tan\varphi_i - c_{n,i}, \text{ where } i = 1,..,n_{p0}; \quad (1)$$

$$f_i^t = \sigma_{n,i} - \sigma_{t0,i}, \text{ where } i = 1,..,n_{p0}, \quad (2)$$

where $n_{p0} \le 3$ is the specific orientation considered;

[3] Forty Kronshtadskoĭ kreposti – shedevry rossiĭskogo inzhenernogo dela pervoĭ poloviny XIX v. [The forts of the Kronstadt Fortress are masterpieces of Russian engineering in the first half of the 19th century]. [Online] URL: https://youtu.be/vjlP8JxezHk?si=W-f2NJ3NrvxOagfw (reference date: 24.06.2024).

[4] Яндекс.Карты [Online]. URL: https://yandex.ru/maps/-/CDGOI-LS (reference date: 24.06.2024).

i – crack orientation number;

$\tau_{s,i}$ – shear stresses, acting along i-th direction;

$\sigma_{n,t}$ – normal stresses, acting perpendicular to i-th direction;

φ_i – friction angle in the i-th direction;

$c_{0,i}$ – cohesion in the i-th direction;

$\sigma_{t0,i}$ – tensile strength in the i-th direction,

where $\sigma_{t0,i} < c_{0,i} \cot \varphi_i$.

Similarly, it is possible to describe the behavior of masonry structures composed by solid blocks (bricks) and weakening surfaces (mortar joints). JRM well describes the behavior of masonry in the horizontal joint plane orientation (direction 2) (Fig. 5). However, unlike the rock mass, masonry tends to have a well-defined, chessboard structure. Thus, in the vertical direction (direction 1) (Fig. 5) there is an additional grip between the surfaces of the blocks. As a result, the tensile and shear strength of the masonry increases along the interconnected section (interlocking effect).

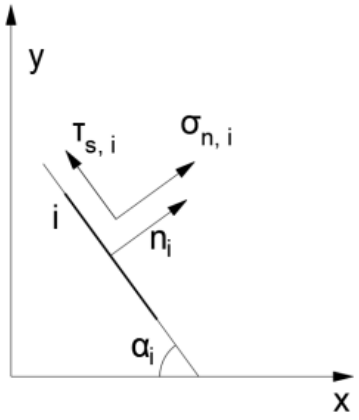

Figure 4. Global and local coordinate systems in 2D conditions [27].

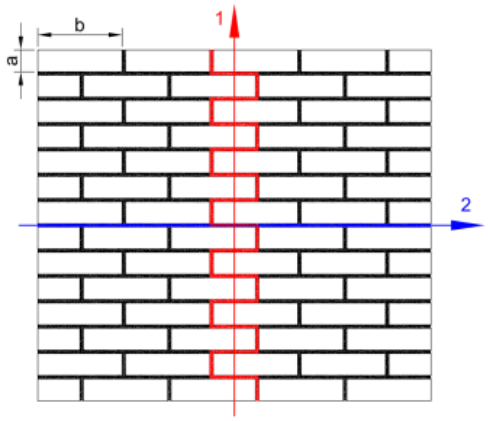

Figure 5. Definition of plane 1 and plane 2 in JMM [27].

Considering masonry in general, it is worth noting its heterogeneity, which is that the material of bricks and mortar are characterized by different deformation properties. The lateral extension of a brick blocks is much smaller than that of mortar for the same stress acting values. As a result, during the deformation of the masonry, the more intense lateral expansion of the mortar will cause additional tensile stresses in the bricks due to the strong cohesion between the brick block and the mortar. This effect increases with a decrease of the mortar grade [55, 56].

On Fig. 6*a* the section of wall made of bricks with height a and length b is shown. As the stress σ_2 increases, the fragment of the wall sustains longitudinal strains, most of which are realized by deformations of the mortar due to its high deformability. The longitudinal mortar strains are accompanied with lateral strains, which are constrained by the bricks above and below (more precisely by cohesion and internal frictional forces between the mortar and the bricks). As a result, tensile stresses σ_1 will arise in the bricks. This effect is increased because of the different values of the lateral extension.

Each brick is under compression stress $\sigma_{n,2} = \sigma_2$, acting perpendicularly to the plane of the horizontal mortar joints, also the bricks are under tensile stress $\sigma_{n,1} \leq \sigma_1$ acting perpendicularly to the plane of the vertical joints and tangential stress $\tau_{s,2}$ acting in the plane of the horizontal joints, as shown in Fig. 6*b*. The stress $\tau_{s,2}$ is due to friction between the bricks and mortar and has an opposite sign relative to the central vertical axis.

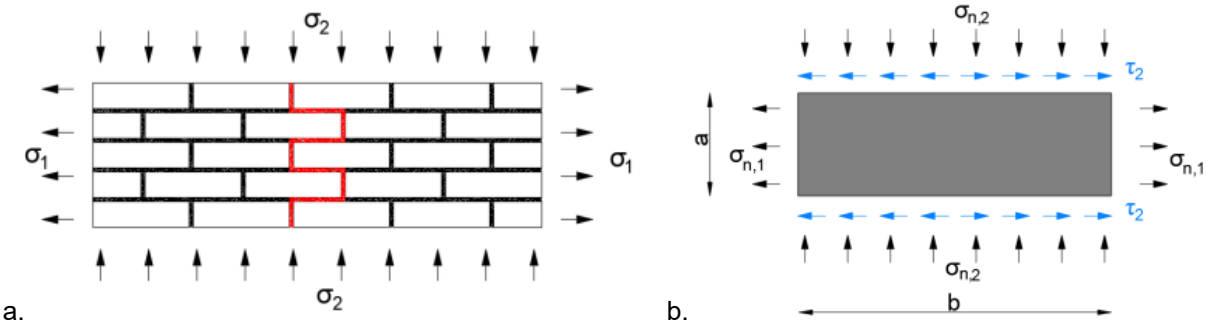

Figure 6. Stress state acting on: a) a part of the masonry wall [27]; b) the single block [27].

To consider the effect of grip between the brick halves, see Fig. 6*a*. Using the failure criteria described in equations (1) and (2), the tensile strength $\sigma_{t,1}$ in plane 1 can be rewritten as:

$$\sigma_{t,1} = \sigma_{t0,1} + \frac{n}{h}(c_{0,2} - \sigma_{n,2}\tan\varphi_2)\frac{b}{2}, \tag{3}$$

where h is the height of the part of the wall, while n is the corresponding number of bed joints.

The height of the block joint can be written as:

$$a = \frac{h}{n}. \tag{4}$$

Using equation (4), equation (3) can be rewritten in the following form:

$$\sigma_{t,1} = \sigma_{t0,1} + \frac{b}{2a}c_{0,2} - \frac{b}{2a}\sigma_{n,2}\tan\varphi_2. \tag{5}$$

The first term of equation (5) is the contribution of the tensile strength $\sigma_{t0,1}$ in plane 1, the second term includes the contribution of cohesion $c_{0,2}$ between the joints in plane 2, and the third term represents the contribution of frictional forces $\tan\varphi_2$ along horizontal joints under the action of compressive stresses $\sigma_{n,2}$.

If we abandon the effect of grip between the bricks in plane 2, i.e., remove the modification of the original JRM, then the tensile stresses will be equal:

$$\sigma_{t,1} = \sigma_{t0,1}. \tag{6}$$

Thus, it follows from equation (6) that the tensile stresses will be the same as the tensile strength $\sigma_{t0,1}$ along the vertical joints.

In turn, the grip effect between the bricks leads to an expansion of the yield surface and an increase in tensile strength. The increase in tensile strength in plane 1 involves a corresponding increase in the existing cohesion (Fig. 7).

$$c_1 = c_{0,1} - \left(\frac{b}{2a}\sigma_{n,2}\tan\varphi_2 - \frac{b}{2a}c_{0,2}\right)\tan\varphi_1. \tag{7}$$

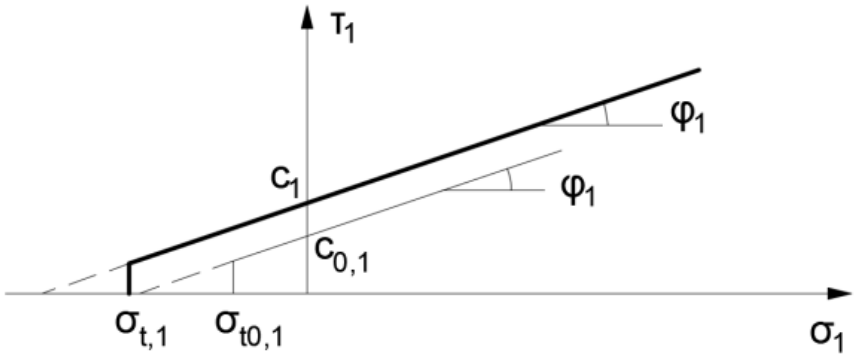

Figure 7. Modified Mohr-Coulomb criterion [27].

Thus, in the formulation of JMM for cohesion forces (7), the effect of interlocking blocks is considered by a new parameter defined as follows:

$$\beta = \tan\varphi_2 \frac{b}{2a}. \tag{8}$$

That coefficient (8) is a function of the dimension ratio of the bricks, while the ratio between the tensile and shear strength is constant.

Equations (5) and (7) can be rewritten as:

$$\sigma_{t,1} = \sigma_{t0,1} - \beta\sigma_{n,2} + c_{0,2}\frac{\beta}{\tan\varphi_2}; \tag{9}$$

$$c_1 = c_{0,1} - \left(\beta\sigma_{n,2} - c_{0,2}\frac{\beta}{\tan\varphi_2}\right)\tan\varphi_1. \tag{10}$$

It should be noted that in JMM, masonry is considered as a continuous medium, so material failure can occur at any point in the area of interest.

Modern masonry structures are characterized by higher tensile strength and cohesion at vertical joints, while old masonry has weak strength and cohesion, near to zero, as a result of mortar degradation at joints. Under such conditions, it is possible to ignore the strength components related to tearing and cohesion.

Then equations (9) and (10) can be rewritten as:

$$\sigma_{t,1} = -\beta\sigma_{n,2}; \tag{11}$$

$$c_1 = -\beta\sigma_{n,2}\tan\varphi_1. \tag{12}$$

Thus, equations (11) and (12) describe the case of complete mortar degradation in masonry. Since in the horizontal direction (direction 2) there is no grip effect between the bricks, the strength parameters in JMM, relative to JRM, are unchanged. As a result, direction 2 is the weakest when loads are applied.

As mentioned previously, JMM can specify up to three sliding directions. Two of them are typically used to specify the masonry pattern. The direction of the sliding surface is described by the angle of incidence α_1 and the angle of rotation α_2. The angle α_1 is defined by turning the sliding plane around the x-axis clockwise; the angle α_2 is defined by turning the sliding plane around the z-axis, counterclockwise. For masonry, a properly defined pattern is set according to the scheme in Fig. 8.

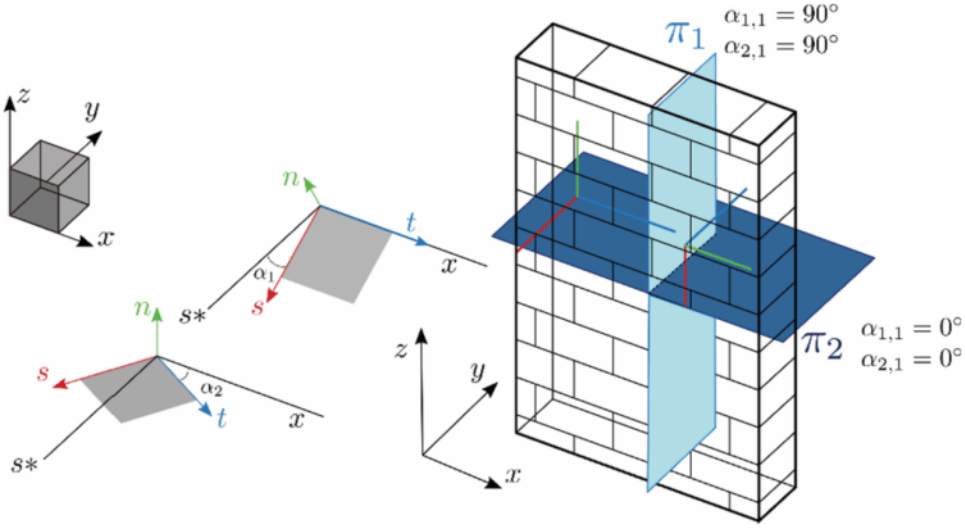

Figure 8. JMM bed and head joint plane orientation [27].

Thus, to describe the strength parameters of the masonry using JMM, it is necessary to find the following set of strength parameters:

c_b – cohesion of the brick block;

φ_b – friction angle of the brick block;

ψ_b – dilatancy angle of the brick block;

$\sigma_{b,t}$ – tensile strength of the brick block;

c_m – shear cohesion of the mortar;

φ_m – friction angle of the mortar;

ψ_m – dilatancy angle of the mortar;

$\sigma_{m,t}$ – normal cohesion of the mortar;

a – block height;

b – block width.

2.2.2. Elastic parameters of the model

It is assumed that the macroscopic structure of the masonry is a homogeneous anisotropic medium where the movement of blocks is replaced by the average movement of the homogenized medium. The general behavior of the medium is calculated with adequate accuracy without considering the motion of each individual block.

In addition to the strength parameters, JMM also considers the isotropic elasticity of the masonry due to the shear modulus G and Poisson's ratio ν. When the deformation parameters of bricks and mortar are available separately, the homogenization procedure of the parameters [57] converts to the equivalent parameters of the masonry. These parameters describe the general behavior of the masonry in the elastic zone.

The shear modulus is given by equation (13), and the Poisson's ratio ν is calculated as an average between ν_{12} and ν_{21}, calculated from equation (14):

$$\frac{1}{G}=\frac{1}{aK_t}+\frac{4a}{b^2K_n+4abK_t}+\frac{1}{\mu_b}; \quad (13)$$

$$\frac{\nu_{12}}{E_1}=\frac{\nu_{21}}{E_2}+\frac{\lambda_b}{2(3\mu_b\lambda_b+\mu_b^2)}. \quad (14)$$

The normal joint stiffness K_n is given by equation (15), the shear joint stiffness K_t – by equation (16),

$$K_n=\frac{E_bE_m}{t_m(E_b-E_m)}; \quad (15)$$

$$K_t=\mu_b\mu_m\frac{1}{t_m}\frac{1}{\mu_b-\mu_m}. \quad (16)$$

The Lame's coefficients are calculated by equations (17) and (18),

$$\mu_b=\frac{E_b}{2(1+\nu_b)}; \quad (17)$$

$$\lambda_b=\frac{\nu_bE_b}{(1-2\nu_b)(1+\nu_b)}. \quad (18)$$

The Young's moduli of masonry are calculated as arithmetic mean of Young's moduli values head E_1 and bed E_2 (19), (20):

$$\frac{1}{E_1}=\frac{1}{aK_n}+\frac{1}{4\mu_b}+\frac{\lambda_b+2\mu_b}{4(3\mu_b\lambda_b+2\mu_b^2)}; \quad (19)$$

$$\frac{1}{E_2}=\frac{4a}{4abK_n+b^2K_t}+\frac{1}{4\mu_b}+\frac{\lambda_b+2\mu_b}{4(3\mu_b\lambda_b+2\mu_b^2)}. \quad (20)$$

Thus, to specify the elastic parameters of the masonry as a homogeneous continuum medium, the following set of parameters should be determined:

E_b – Young's modulus of brick;

E_m – Young's modulus of mortar;

ν_b – Poisson's ratio of brick;

ν_m – Poisson's ratio of mortar.

2.3. Getting Input Model Parameters according to the Results of Laboratory Tests

The program of mechanical compression tests is standard for similar materials and is described in the Russian regulatory literature (GOST R 58767-2019 "Mortars. Test methods using reference specimens" and GOST R 58527-2019 "Wall materials. Methods for determination of ultimate compressive and bending strength"). Based on the uniaxial compression tests performed, the peak strength of bricks and mortar are defined. Obtained data is used to calculate the average parameters of the masonry. Then, in accordance with the Russian regulatory documents, the values of normal and shear cohesion of the mortar are determined.

Tests were also performed on cylindrical specimens drilled out of bricks for uniaxial and triaxial compression tools (TXT) using techniques similar to those used for laboratory rock testing.

For this purpose, samples of brick and masonry mortar were taken from the walls of the workshop buildings. The extraction of masonry fragments was carried out in three sites on each floor of the building

(Fig. 11). 15 brick samples were collected. During sampling, it was found that during construction, bricks from several manufacturers were used. A large textural heterogeneity of the samples was observed. This phenomenon is directly related to the features of the ceramic brick production in the 19th century, namely the imperfection of the technology of forming bricks, which led to the formation of imperfect texture.

The rest of load-bearing elements: floor beams, slab floor, foundations – were specified by a linear-elastic model. To specify the slab material, concrete samples were extracted from cemented crushed bricks and used for uniaxial compression test (UCT).

2.3.1. Laboratory methodology for brick material

UCT were carried out in accordance with prescribing displacements, with loading speed not exceeding 0.5 mm/min, full mythology described in Russian State Standard GOST 21153.2-84 “Rocks. Methods for determination of axial compression strength”, and TXT – in accordance with GOST 21153.2-84 “Rocks. Method for determination of triaxial compressive strength”. All tests were carried out on SPGU, Toni Hendrick and MTS 816 Rock Test System presses.

Selected bricks were dried for two months at room temperature in a non-ventilated dry room. After drying, some of the bricks were prepared for testing. According to the methodology, the selected bricks were divided into two halves. The beds of each brick were smoothed with gypsum mortar with grade G5 (Fig. 9) and laid bedded on top of each other.

Figure 9. Brick samples prepared for UCT, compiled by the authors.

For extra alignment, cardboard sheets of up to 1 cm thick were placed between the brick beds.

From the stretcher faces of the rest bricks, cylindrical core samples were drilled for UCT and TXT. The result of drilling and the final look of the specimens are shown in Fig. 10.

Figure 10. Cylindrical samples prepared for TXT and UCT, compiled by the authors.

The surfaces of the cylinder specimens were grinded, and visual defects on the surface were “cured” with plasticine.

To construct failure line of the bricks, in addition to UCT, 3 series of tests with different values of lateral compression were performed. Lateral compression varied in the range from 2 to 6 MPa with step of 2 MPa.

2.3.2. Laboratory methodology for mortar material

The test program for mortar joint material included testing cubic samples of 20–40 mm under uniaxial compression according to the methodology described earlier. To make the mortar samples of the desired size, large pieces were removed from the masonry and cut into 20–40 mm square plates. Then two plates were cemented together with a layer of gypsum paste 1–2 mm thick and G5 grade. Top and bottom surfaces were also smoothed with a thin layer of gypsum. Fig. 12 shows the final views of the specimens before testing.

Figure 11. Samples of wall and floor materials, compiled by the authors.

Figure 12. Mortar samples prepared for testing, compiled by the authors.

2.4. Creating numerical model for verification

As a part of the restoration work of this object, measurements of cumulative unequal settlements and building tilt were made. Fig. 13 shows a profile of measuring the cumulative unequal settlements of the building. The largest differential settlement is $i_{max} = 0.015$. Everywhere the vertical walls deviation is observed. The largest detected wall decline is $j_{max} = 0.028$. In general, the wall along A-axis deviates to the "island" side by up to 108 mm. Cross walls also have tilt towards the island, which is demonstrated by the existence of inclined through cracks in them. At the same time, the wall on B-axis (sea facade) remains stable.

Figure 13. Diagram of the accumulated settlements across wall A. The values are given in millimeters[5].

In PLAXIS 3D software package, the numerical simulation of the whole workshop building was performed. In current research, the interaction between soils and foundations of the building is not considered directly. The available results of the survey allow to model in-situ settlements of the foundation footing by specified displacements along it. Fig. 14 represents the general view of the numerical model. To achieve adequate results, the building walls were modeled with mesh coarsners factor equal to 0.07. Thus, the numercial model contains 324675 finite elements. In "staged construction" section three steps were performed sequentially:

1. All building structures were modeled. Displacements along the footings of all foundations in all directions were forbidden.

[5] Forty Kronshtadskoĭ kreposti – shedevry rossiĭskogo inzhenernogo dela pervoĭ poloviny XIX v. [The forts of the Kronstadt Fortress are masterpieces of Russian engineering in the first half of the 19th century]. [Online] URL: https://youtu.be/vjlP8JxezHk?si=W-f2NJ3NrvxOagfw (reference date: 24.06.2024).

2. The computational step required to reach the equilibrium state and set the accumulated strains to zero.

3. The accumulated strains were repeatedly set to zero again, and the diagram of vertical settlements along the base of the foundation of wall A was created.

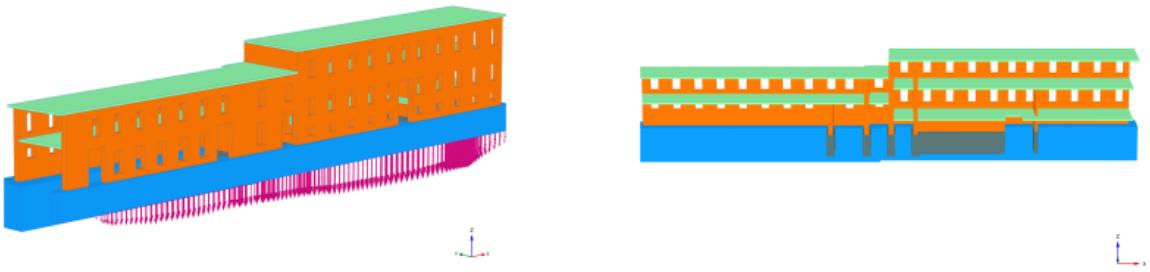

a) b)

Figure 14. Design scheme of the workshop building: a) general view of the design scheme with given displacements; b) sectional drawing of the building, compiled by the authors.

3. Results and Discussion

3.1. Laboratory Tests Results

3.1.1. Obtained mechanical parameters of brick samples

Fig. 15 shows a typical failure mechanism of the half's brick samples. When processing test results, test results that strongly deviated from the sample mean were discarded. Table 1 shows the obtained deformation moduli and uniaxial compression stress of masonry bricks. Fig. 16 shows the obtained stress-strain curves of bricks under uniaxial loading.

Figure 15. General view of the brick samples at failure, compiled by the authors.

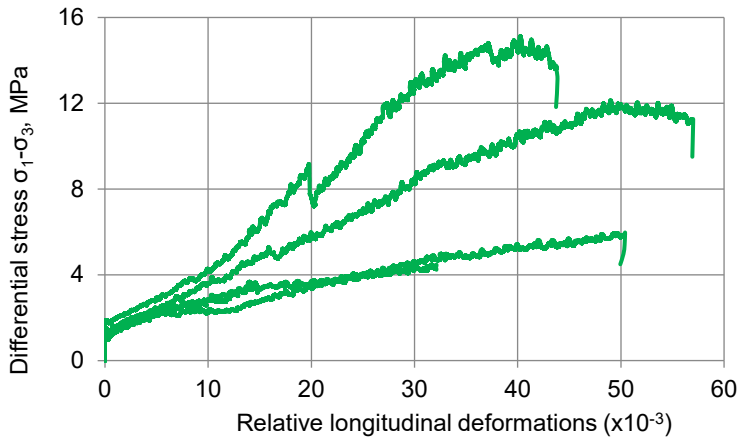

Figure 16. Stress-strain relations curves for brick samples, compiled by the authors.

Table 1. Geometrical properties of brick specimens and test results.

No.	Block length a, mm	Block width b, mm	Block height h, mm	Mass m, g	UCS σ, MPa	Young's modulus E, GPa
1	125	135	147	4675	3.7	0.4
2	115	105	120	2605	4.5	0.3
3	120	100	140	4400	15.1	0.5
4	120	118	155	4640	12.2	0.2
5	125	125	130	4002	6.0	0.1

The failure mechanism of the drilled brick specimens after UCT and TXT shown in Fig. 17, 18.

Figure 17. General view of cylindrical samples at failure after TXT, compiled by the authors.

Figure 18. General view of cylindrical samples at failure after UCT, compiled by the authors.

The received results are characterized by high heterogeneity, therefore, they should be processed with a certain safety factor.

Heterogeneity is probably caused by various manufacturing technology of tested bricks and different sampling sites. Moreover, heterogeneity was observed even in speciments drilled from the same brick, which may reflect the influence of the historical distribution in stress-strain state applying to the brick surfaces and therefore lead to different microfracture formation. In the future, more sophisticated statistical procedures, such as the use of artificial neural networks, should be applied to samples with such heterogeneity [58, 59].

Obtained results allow identifying the dependence between increasing strength limit of bricks with growing lateral compression. Fig. 19 shows the final set of stress-strain curves.

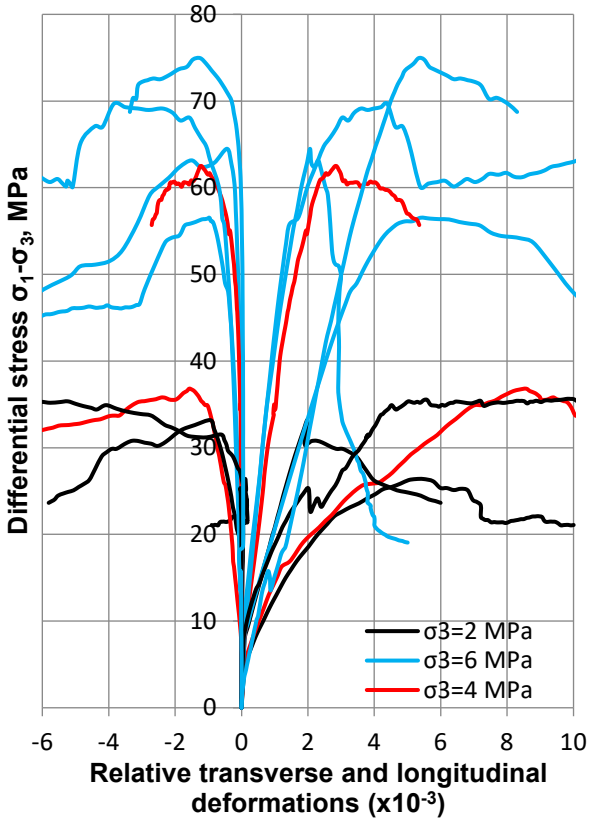

Figure 19. Stress-strain relations curves for brick cylindrical samples, compiled by the authors.

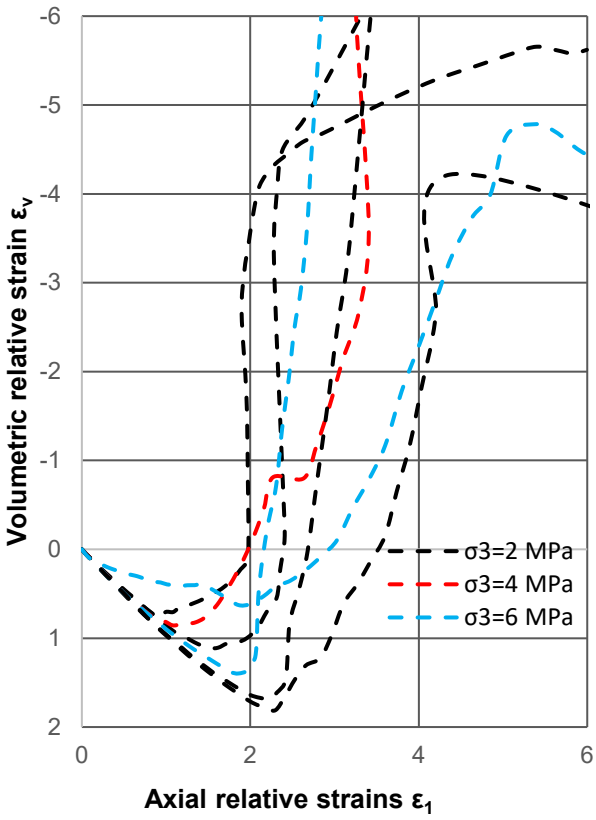

Figure 20. Curves representing the dependence of volumetric strains versus axial strains, compiled by the authors.

Analysis the obtained data shows the influence of the scale effect on the test results [60], because uniaxial compression stress (UCS) of brick parts is much lower than that USC of cylindric samples. The average UCS of bricks parts is 8.28 MPa, while the average UCS of cylinder specimens is 18.77 MPa. Thus, the ratio of these values may give a scale factor k equal to 0.44. The indicates and influence of the scale effect on the test results for bricks is given in [61, 62]. The coefficient k is used in further to reduce the strength limits and deformation moduli. The resulting parameters are presented in Table 2.

Table 2. Geometrical properties of brick cylindrical specimens and test results decreases by k.

Site location	Sample number	Diameter d, mm	Height h, mm	Mass m, g	Lateral pressure σ_3, MPa	Volume strength $k \cdot \sigma_v$, MPa	Young's modulus $k \cdot E$, GPa	Poisson's ratio ν
1	1	39.9	93.4	196.8	2	12.52	3.54	–
	2	39.9	93.3	201.9	4	17.99	3.42	0.274
	3	39.8	82.5	192.1	2	15.51	7.44	0.136
	4	39.9	94.8	224.3	6	27.57	6.07	0.254
2	5	39.8	94.8	266.7	6	31.07	15.98	0.080
	6	39.8	93.0	243.1	0	8.93	2.27	–
3	7	39.9	87.8	246.9	4	29.30	14.75	0.104
	8	39.8	87.4	249.2	6	33.37	18.42	0.310
	9	39.8	85.2	249.8	2	16.59	5.89	0.008
	10	39.9	93.2	256.4	6	35.68	6.76	–
	11	40.0	92.8	191.4	0	9.25	1.35	–
	12	39.6	92.1	189.6	0	7.71	1.79	–
	13	39.9	69.5	145.1	0	9.82	1.70	–
	14	39.1	91.3	210.3	0	5.67	1.50	–

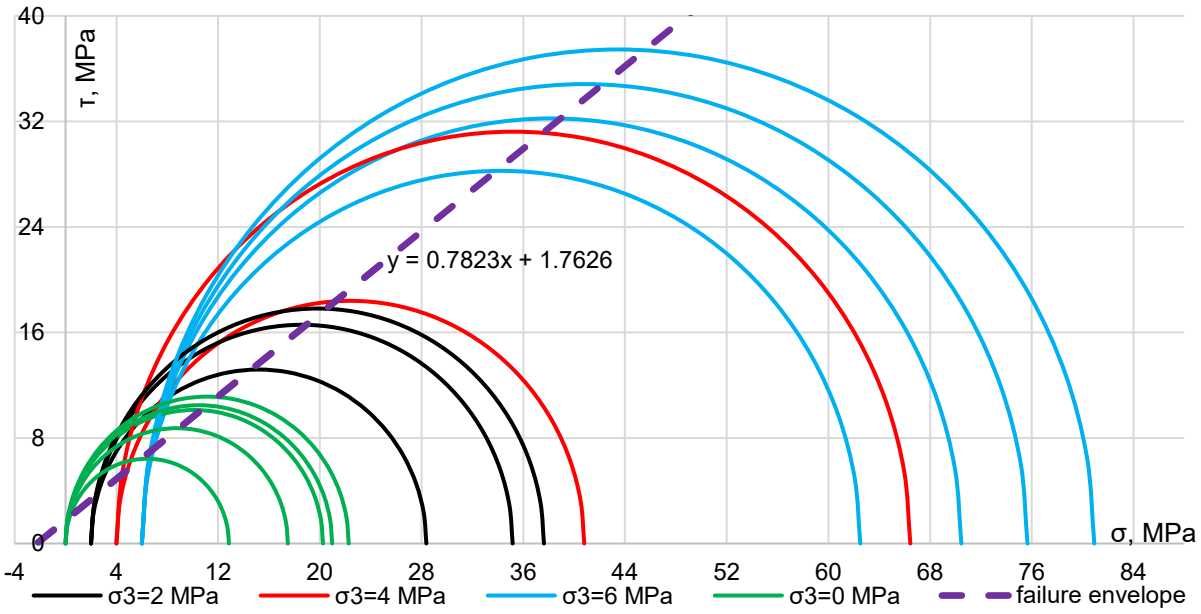

Figure 21. Mohr's circles for UCT and TXT and Mohr-Coulomb failure envelope, compiled by the authors.

From the obtained failure line of the brick (Fig. 21) the value of the internal friction angle of the material $\varphi_b = 38°$, cohesion $c_b = 1.17$ MPa were defined.

From TXT curves for dependency volume strain versus axial strain $\varepsilon_1 - \varepsilon_2$ are plotted. This graph is shown in Fig. 20.

The obtained data illustrates changing signs of volumetric deformations, which means the dilatancy existence with an attenuated character. Using equation (21) proposed by Vermeer and De Borst [63], the average value of the dilatancy angle for each sample are calculated.

$$\psi = \arcsin\left(\frac{\Delta\varepsilon_v}{\Delta\varepsilon_v - 2\Delta\varepsilon_1}\right), \quad (21)$$

where $\Delta\varepsilon_v$ – volumetric strain increment; $\Delta\varepsilon_1$ – axial strain increment.

Depending on the chosen range for any curves, the dilatancy angle takes values differing from the angle of internal friction by $\pm 5°$ in both directions. Therefore, the dilatancy angle was taken to be equal to the angle of internal friction $\psi_b = 38°$. In this case, an associated law of plastic flow rule is valid for the brick material.

The tensile strength was defined by two methods. First one is geometrical, by plotting the Mohr-Coulomb failure line in the tensile zone. The second method from tabulated data in Russian regulatory documents, according to which $\sigma_{t,mc}$ equals 200 or 180 KH/m², depending or brick grade. Grades where defining during building survey.

In the homogenization procedure of elastic parameters for masonry, the average value of the deformation modulus from results of UCT equal to $E_b = 1722$ MPa, was used. The lateral stain coefficient (Poisson's ratio) based on TXT defined as $\nu_b = 0.17$.

3.1.2. Obtained mechanical parameters of mortar material

Table 3 shows the deformation modules and UCS for masonry mortar and the stress-strain curves of the mortar under uniaxial loading.

Table 3. Geometrical properties of mortar specimens and test results and stress-strain relations curves for mortar samples, compiled by the authors.

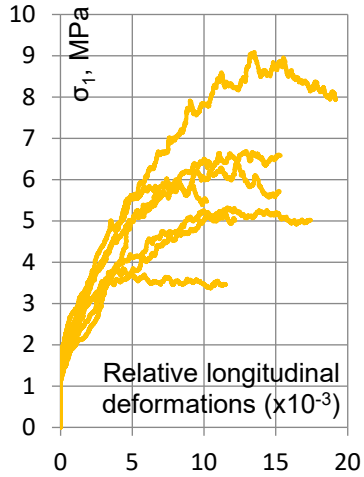

S. num.	Length, a, mm	Width b, mm	Height h, mm	Mass m, g	Volume strength σ_v, MPa	Young's modulus E, GPa
1	29.0	36.0	42.0	95.3	9.09	0.56
2	35.0	40.0	33.0	95.3	6.69	0.62
3	38.0	40.0	44.0	150.8	6.25	0.75
4	37.0	40.0	56.0	187.0	5.35	0.37
5	35.3	40.0	38.0	108.6	6.41	0.61
6	40.0	36.0	53.0	158.6	3.93	0.66
7	40.0	40.0	37.5	125.0	5.45	0.49

In the homogenization procedure of elastic parameters for masonry, the average value of the deformation modulus equal to $E_m = 556.1$ MPa, was used. The lateral strain coefficient, based on data from [39, 40], was assumed to be $\nu_m = 0.25$ with the ratio $\frac{\sigma}{R} = 0.6$, where R is the ultimate compressive strength of the mortar.

3.2. Summurised Input Parameters for JMM and Numerical Simulation

The structures of the foundation, walls and slabs are implemented as three-dimensional elements. The slab beams are made in the form of ideal-elastic wire elements. For the walls, 2 sets of input parameters were considered (see w.1 and w.2 in Table 4). First set included lab test data and scientific research materials. Second set was based on tabulate data in Russian regulatory documents. The input JMM

parameters are presented in Tables 4, 5. An elastic model was adopted for the floor beams, with the input parameters in Table 6.

Within the framework of scientific and educational work, it was not possible to obtain all necessary parameters of adhesion and the angle of internal friction of the solution; the results of studies were used to set them [46–49]. The dilatancy angle was taken to be equal to the angle of internal friction. In this case, an associated law of plastic flow rule is valid for the mortar material.

Table 4. Input parameters of masonry walls for JMM.

Material	w.1	w.2	
	a, b	*a*	*b*
γ, kH/m^3	19.7	19.7	19.7
G, kH/m^2	4.58E05	8.00E05	6.18E05
ν	0.19	0.2	
c_{mc}, kH/m^2	1760	800	650
φ_{mc}, °		38.04	
ψ_{mc}, °		38.04	
$\sigma_{t,mc}$, kH/m^2	1350	200	180
SF_{beta}		1.07	
$a_{1,1}$, °		90	
$a_{1,2}$, °		90	
c_i, kH/m^2	160	160	
φ_i, °		30	
ψ_i, °		30	
$\sigma_{t,i}$, kH/m^2	140	80	
$a_{2,1}$, °		0	
$a_{2,2}$, °		0	

Table 5. Input parameters of foundations and slabs for Linear Elastic model.

Material	Foundation	Foundation of internal walls	Floor
γ, kH/m^3	20	20	20
E_{ref}, kH/m^2	13.00E6	0.80E6	8.826E6
ν		0.2	

Table 6. Input parameters of flor beams for Linear Elastic model.

Material	I-beam profile N18	I-beam profile N26
γ, kH/m^3	78	78
A, m^2	2.790E-3	5.340E-3
I_2, m^4	0.01450E-3	0.05740E-3
I_3, m^4	0.8730E-6	2.880E-6
E_{ref}, kH/m^2	210.0E6	210.0E6

3.3. Numerical Simulation Results and Comprasion with Survey Data

In PLAXIS 3D two calculation situations were considered, namely (a, b) by used sets of masonry materials (Table 4, 8). In addition, two more calculation scenarios were considered, so in models *a* and *c* masonry materials were used considering the associated plastic flow rule. In models *b* and *d* materials without regard to dilatancy were used (Table 8). Thus, 4 calculations with different sets of input parameters to JMM were performed. The results of a set of laboratory tests on bricks correlate with the results obtained by other authors [36, 38]. The obtained parameters of JMM adequately correlate with the input parameters accepted by other researchers [27, 64].

Fig. 22 shows the results of the building survey with the defects applied to wall A. The numerical modeling results are shown in Fig. 23–25. It can be noted that the shear strains presented in Fig. 23 with a good reliability are formed in the same places as observed wall defects. Cracks are concentrated at the lintels above the window and door openings in the left and right parts of the facade. There is also a detachment of the cornice under the building's roof. The nature of the distribution, the angle of inclination, and the direction of development indicate the sedimentary nature of their occurrence, which is confirmed by the results of numerical calculations.The similarity of the survey and numerical results indicates that there is a visual qualitative convergence between the behavior of real masonry structures and those predicted by the numerical model based on JMM.

It may be concluded that mostly cracks in the building facade are formed as a result of irregular settlement of the building foundations. The obtained result demonstrated the effectiveness of JMM for predicting the development of cracks in historic masonry buildings.

It should be noted that a set of tools PC PLAXIS 3D can not fully describe the interaction of different structural elements of the building, which leads to distorted simulation results.

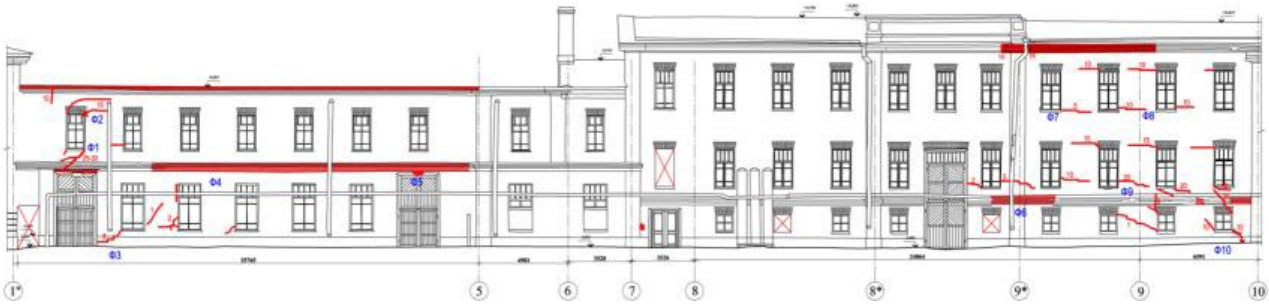

Figure 22. Scheme of building facade defects[6].

Comparing calculation results for two input parameters set indicates the observed qualitative similarity of deforming processes in the masonry. Second input parameters set (calculations *c* and *d*), which used tabulated data in Russian regulatory documents, show widespread development of tension zones (Fig. 24), due to lower (almost two times) tensile strength of normal cohesion of mortar and lower (seven times) tensile strength of bricks. The tensile strength of the bricks was intentionally decreased to demonstrate a further failure process in the tensile stress zones. At the same time, for *c* and *d* input parameters set an additional increase of plastic strains in the compression zones was also observed. In the right and left lower corners of the building, the compressive loads have such magnitude that reaching the strength limit and material failure occurs (red points in Fig. 24*c*), which is practically not observed in the scenario *a*.

Numerical results derived with input parameters for JMM based on tabulated data lead to a more conservative solution and include relatively large fracture zones. Thus, the parameters according to the scenario c enable to consider the worst-case scenario for this problem conditions.

The dilatancy angle determines the direction of the plastic potential vector with respect to the Mohr-Coulomb yield surface. As a consequence, dilatancy is responsible for the proportional relation between plastic volume strains and plastic shear strains. Thus, if $\psi = 0^\circ$, as it was assumed in calculations (*b, d*), volumetric strains occur only under the volume compression stress paths, see Fig. 25 (*b, d*), while shear strains develop more intensively, see Fig. 23 (*b, d*). For cases where $\psi = \varphi$, extra volumetric deformations occur in zones where stresses level exceed Mohr-Coulomb failure criterion, as is shown in Fig. 25 (*a, c*) and Fig. 23 (*a, c*).

The presence of dilatancy affects the angle of inclination of the formed zones of shear deformations (or zones of crack development) from window openings, in relation to the horizon, which is especially evident in the right side of the building (Fig. 23). Also, the location of cap and hardening points is changed (Fig. 24).

Both cases of flow rule, associated and no-associated, are presented in the paper.

[6] Forty Kronshtadskoĭ kreposti – shedevry rossiĭskogo inzhenernogo dela pervoĭ poloviny XIX v. [The forts of the Kronstadt Fortress are masterpieces of Russian engineering in the first half of the 19th century]. [Online] URL: https://youtu.be/vjlP8JxezHk?si=W-f2NJ3NrvxOagfw (reference date: 24.06.2024).

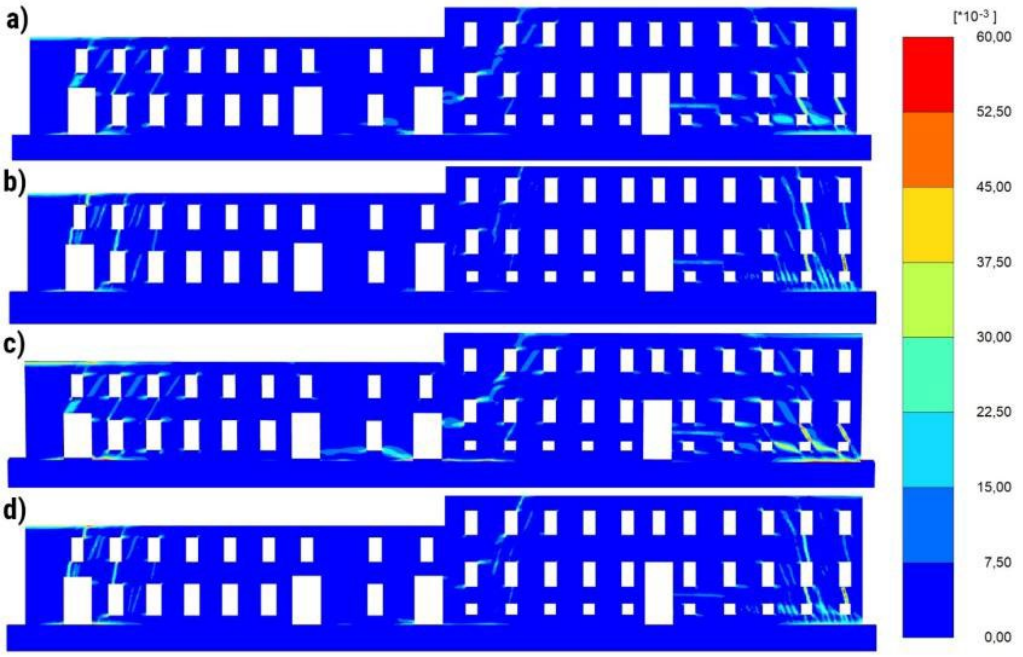

Figure 23. Achieved shear strains after applying defined displacements, compiled by the authors.

The diagrams showing the zones of crack formation and development during nonuniform building settlement correlate with the diagrams obtained by the model developers [27, 28], other researchers [8] and by comparing the simulation results with discrete [64] and other [14] approaches.

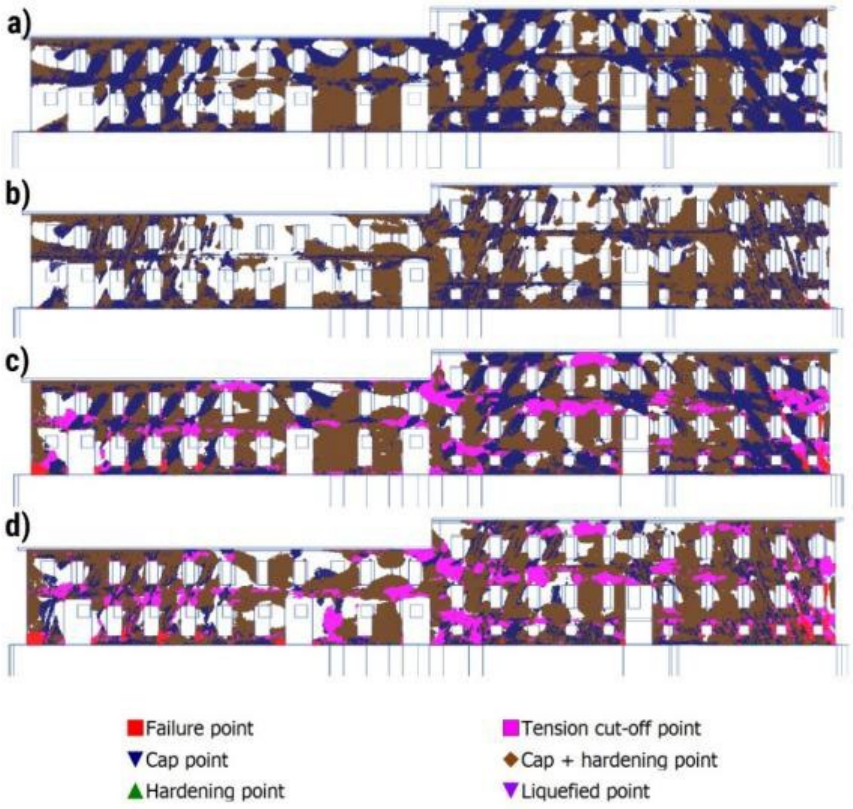

Table 8. Considered calculation scenarios.

Case	Input parameters by:	Dilatancy
a	laboratory	$\psi = \varphi$
b	laboratory	$\psi = 0°$
c	tablulated data	$\psi = \varphi$
d	tablulated data	$\psi = 0°$

Figure 24. Achieved plastic points after applying defined displacements, compiled by the authors.

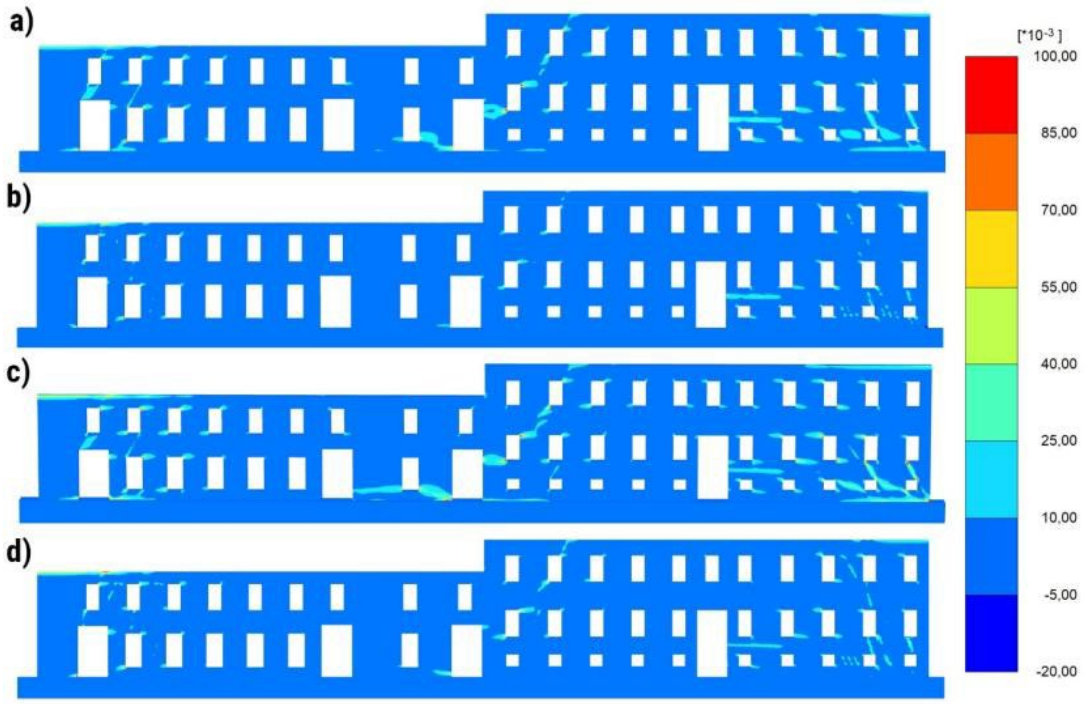

Figure 25. Achieved volume strains after applying defined displacements, compiled by the authors.

4. Conclusions

A set of laboratory tests was carried out, strength and deformation properties of historic bricks and masonry were obtained. To determine the mechanical behavior of bricks under triaxial stress state, a new method of laboratory testing was proposed - by drilling cylindrical specimens from the brick body. A method for obtaining JMM input parameters based on uniaxial tests of mortar and bricks and triaxial tests of bricks was proposed.

It was found that the parameters thus obtained were sufficient to determine the mechanical behavior of historic brick masonry using JMM. The principle of JMM operation was demonstrated on the example of a historic brick building constructed in the beginning of the 20th century. Numerical modeling of the main load-bearing structures of the building was carried out, considering the subsidence of its foundation part. Based on the results of the study, the following conclusions were obtained:

1) The JMM qualitatively described the processes of crack formation with a high degree of reliability, which indicated the possibility of verifying the obtained input parameters of JMM in a similar way.

2) The parameters of brickwork obtained as a result of tests adequately described the process of deformation of a real structure. Further refinement of the test methodology is required. Emphasis should be placed on the scale effect that occurs when testing brick samples. This phenomenon significantly affects the resulting masonry input parameters.

3) A large heterogeneity of the mechanical properties of the tested samples should be noted, which leads to a distortion of the final values of the parameters. More extensive research is required in this direction.

4) When modeling masonry with parameters from tabulated data, more conservative solution was obtained. The formation of zones with excess tensile strength was observed, which was related to the tensile strength of the brick material.

5) Relatively closer agreement with the survey results was achieved when the input parameters for JMM were obtained from lab tests of the bricks, in this way it is possible to verify the input parameters of the JMM model.

6) Calculations considering dilatancy better present the distribution of volumetric deformations in the zones of crack initiation. Based on the received results, it was difficult to conclude which version of flow rule better describe survey findings.

The results allow to conclude that numerical simulation of historic brick buildings can be used as well as their surveys, which will make it possible to clarify the positions of crack development zones in hard-to-reach places and/or in places which was missed during the surveys.

The methodology for determining JMM input parameters is particularly relevant for cases where large-scale testing with sections of old masonry structures is not possible. The considered approach has the prospect of being used to describe the further state of the brickwork during aging by setting an increased differential settlement of the walls of the building.

References

1. Angelillo, M. Constitutive relations for no-tension materials. Meccanica. 1993. 28(3). Pp. 195–202. DOI: 10.1007/bf00989121
2. Nazir, S., Dhanasekar, M. Modelling the failure of thin layered mortar joints in masonry. Engineering Structures. 2013. 49. Pp. 615–627. DOI: 10.1016/j.engstruct.2012.12.017
3. Nazir, S., Dhanasekar, M. A non-linear interface element model for thin layer high adhesive mortared masonry. Computers & Structures. 2014. 144. Pp. 23–39. DOI: 10.1016/j.compstruc.2014.07.023
4. de Buhan, P., de Felice, G. A homogenization approach to the ultimate strength of brick masonry. Journal of the Mechanics and Physics of Solids.1997. 45(7). Pp. 1085–1104. DOI: 10.1016/S0022-5096(97)00002-1
5. Cecchi, A., Sab, K. A multi-parameter homogenization study for modeling elastic masonry. European Journal of Mechanics – A/Solids. 2002. 21(2). Pp. 249–268. DOI: 10.1016/S0997-7538(01)01195-0
6. Zucchini, A., Lourenço, P.B. A micro-mechanical model for the homogenisation of masonry. International Journal of Solids and Structures. 2002. 39(12). Pp. 3233–3255. DOI: 10.1016/S0020-7683(02)00230-5
7. Marfia, S., Sacco, E. Multiscale damage contact-friction model for periodic masonry walls. Computer Methods in Applied Mechanics and Engineering. 2012. 205–208. Pp. 189–203. DOI: 10.1016/j.cma.2010.12.024
8. de Felice, G., Malena, M. Failure pattern prediction in masonry. Journal of Mechanics of Materials and Structures. 2019. 14(5). Pp. 663–682. DOI: 10.2140/jomms.2019.14.663
9. Kapustin, S.A., Likhacheva, S.Iu. Modelirovanie protsessov deformirovaniia i razrusheniia materialov s periodicheski povtoriaiushcheĭsia strukturoĭ [Modeling the processes of deformation and destruction of materials with a periodically repeating structure]. Nizhniy Novgorod: NNGASU, 2012. 96 p.
10. Anthoine, A. Homogenization of periodic masonry: plane stress, generalized plane strain or 3D modelling? Communications in numerical methods in engineering. 1997. 13(5). Pp. 319–326. DOI: 10.1002/(sici)1099-0887(199705)13:5<319::aid-cnm55>3.0.co;2-s
11. Massart, T., Peerlings, R., Geers M., Gottcheiner, S. Mesoscopic modeling of failure in brick masonry accounting for three-dimensional effects. Engineering Fracture Mechanics. 2005. 72(8). Pp. 1238–1253. DOI: 10.1016/j.engfracmech.2004.09.007
12. Milani, G., Lourenço, P.B., Tralli, A. Homogenised limit analysis of masonry walls. Part I: failure surfaces. Computers & Structures. 2006. 84(3). Pp. 166–180. DOI: 10.1016/j.compstruc.2005.09.005
13. Livesley, R.K. Limit analysis of structures formed from rigid blocks. International Journal for Numerical Methods in Engineering. 1978. 12(12). Pp. 1853–1871. DOI: 10.1002/nme.1620121207
14. Portioli, F., Casapulla, C., Gilbert, M., Cascini, L. Limit analysis of 3D masonry block structures with non-associative frictional joints using cone programming. Computers & Structures. 2014. 143. Pp. 108–121. DOI: 10.1016/j.compstruc.2014.07.010
15. Malena, M., Portioli, F., Gagliardo, R., Tomaselli, G., Cascini, L., de Felice, G. Collapse mechanism analysis of historic masonry structures subjected to lateral loads: a comparison between continuous and discrete models. Computers & Structures. 2019. 220. Pp. 14–31. DOI: 10.1016/j.compstruc.2019.04.005
16. Karasev M.A., Petrushin V.V., Rysin A.I. The hybrid finite/discrete element method in description of macrostructural behavior of salt rocks. MIAB – Mining Informational and Analytical Bulletin. 2023. 4. Pp. 48–66. DOI: 10.25018/0236_1493_2023_4_0_48
17. Belyakov, N., Smirnova, O., Alekseev, A., Tan, H. Numerical Simulation of the Mechanical Behavior of Fiber-Reinforced Cement Composites Subjected Dynamic Loading. Applied Sciences. 2021. 11(3). Article no. 1112. DOI: 10.3390/app11031112
18. Verbilo, P., Karasev, M., Belyakov, N., Iovlev, G. Experimental and numerical research of jointed rock mass anisotropy in a three-dimensional stress field. Rudarsko-geološko-naftni zbornik. 2022. 37(2). Pp. 109–122. DOI: 10.17794/rgn.2022.2.10
19. Liu, G., Houlsby, G.T., Augarde, C.E. 2-dimensional analysis of settlement damage to masonry buildings caused by tunnelling. The Structural Engineer. 2000. 79(1). Pp. 19–25.
20. Amorosi, A., Boldini, D., de Felice, G., Malena, M. Tunnelling-induced deformation on a masonry structure: a numerical approach. Geotechnical aspects of underground construction in soft ground. 2012. Pp. 353–359. DOI: 10.1201/b12748-48
21. Giardina, G., van de Graaf, A.V., Hendriks, M.A.N., Rots, J.G., Marini, A. Numerical analysis of a masonry façade subject to tunnelling-induced settlements. Engineering Structures. 2013. 54. Pp. 234–247. DOI: 10.1016/j.engstruct.2013.03.055
22. Burd, H.J., Houlsby, G.T., Augarde, C.E., Liu, G. Modelling tunnelling-induced settlement of masonry buildings. Proceedings of the Institution of Civil Engineers – Geotechnical Engineering. 2000. 143(1). Pp. 17–29. DOI: 10.1680/geng.2000.143.1.17
23. Pickhaver, J.A., Burd, H.J., Houlsby, G.T. An equivalent beam method to model masonry buildings in 3D finite element analysis. Computers & Structures. 2010. 88(19–20). Pp. 1049–1063. DOI: 10.1016/j.compstruc.2010.05.006
24. Giardina, G., Ritter, S., DeJong, M.J., Mair, R.J. Modelling the 3D brittle response of masonry buildings to tunnelling. Structural analysis of Historical Constructions: Anamnesis, diagnosis, therapy, controls. 2016. Pp. 481–488. DOI: 10.1201/9781315616995-64
25. Burd, H.J., Yiu, W.N., Acikgoz, S., Martin, C.M. Soil-foundation interaction model for the assessment of tunnelling-induced damage to masonry buildings. Tunnelling and Underground Space Technology. 2022. 119. Article no. 104208. DOI: 10.1016/j.tust.2021.104208
26. Yiu, W.N, Burd, H.J., Martin, C.M. Finite-element modelling for the assessment of tunnel-induced damage to a masonry building. Géotechnique. 2017. 67(9). Pp. 780–794. DOI: 10.1680/jgeot.sip17.P.249
27. Lasciarrea, W.G., Amorosi, A., Boldini, D., de Felice, G., Malena, M. Jointed Masonry Model: A constitutive law for 3D soil-structure interaction analysis. Engineering Structures. 2019. 201. Article no. 109803. DOI: 10.1016/j.engstruct.2019.109803

28. Amorosi, A., Sangirardi, M. Coupled three-dimensional analysis of the progressive tunnelling-induced damage to masonry buildings: is it always worth it? Tunnelling and Underground Space Technology. 2021. 118. Article no. 104173. DOI: 10.1016/j.tust.2021.104173
29. Godman, R.E., Taylor, R.L., Brekke, T.L. A model for the mechanics of jointed rock. Journal of the Soil Mechanics and Foundations Division. 1968. 94(3). Pp. 637–659. DOI: 10.1061/JSFEAQ.0001133
30. Amorosi, A., Boldini, D., de Felice, G., Lasciarrea, W.G., Malena, M. Analisi geotecnica e strutturale del Ninfeo di Genazzano. Rivista Italiana di Geotecnica. 2015. 1. Pp. 29–44.
31. Baryakh, A.A., Devyatkov, S.Yu., Denkevich, E.T. Mathematical modelling of displacement during the potash ores mining by longwall faces. Journal of Mining Institute. 2023. 259. Pp. 13–20. DOI: 10.31897/PMI.2023.11
32. Protosenya, A.G., Alekseev, A.V., Verbilo, P.E. Prediction of the stress-strain state and stability of tunnel face at the intersection of disturbed zones of the soil mass. Journal of Mining Institute. 2022. 254. Pp. 252–260. DOI: 10.31897/PMI.2022.26
33. Karasev, M.A., Nguyen, T.T. Method for predicting the stress state of the lining of underground structures of quasi-rectangular and arched forms. Journal of Mining Institute. 2022. 257. Pp. 807–821. DOI: 10.31897/PMI.2022.17
34. Demenkov, P.A., Komolov, V.V. Study of influence of the deep pit construction on soil mass in flat and spatial formulation. MIAB – Mining Informational and Analytical Bulletin. 2023. 6. Pp. 97–110. DOI: 10.25018/0236_1493_2023_6_0_97
35. Perunov, A.S. On the issue of heterogeneity of structural bricks of buildings of historical development. Engineering journal of Don. 2021. 5(77). Pp. 32–44.
36. Chumachenko, N.G., Chmarkova, S.V. To the question of brick laying restoration of old construction buildings. Problemy gradostroitel'noĭ rekonstruktsii [Problems of urban reconstruction]. 2019. Pp. 148–153.
37. Gospodarikov, A.P., Trofimov, A.V., Kirkin A.P. Evaluation of deformation characteristics of brittle rocks beyond the limit of strength in the mode of uniaxial servohydraulic loading. Journal of Mining Institute. 2022. 256. Pp. 539–548. DOI: 10.31897/PMI.2022.87
38. Moayedian, S.M., Hejazi, M. Effect of scale on compressive strength of brick masonry with gypsum mortar. Measurement. 2021. 172. Article no. 108932. DOI: 10.1016/j.measurement.2020.108932
39. Soleymani, A., Najafgholipour, M.A., Johari, A. An experimental study on the mechanical properties of solid clay brick masonry with traditional mortars. Journal of Building Engineering. 2022. 58. Article no. 105057. DOI: 10.1016/j.jobe.2022.105057
40. Kaldar-ool, A-Kh.B., Opbul, E.K. Stress condition of orthotropic vault structure with cylindrical anisotropy. Magazine of Civil Engineering. 2022. 116(8). Article no. 11605. DOI: 10.34910/MCE.116.5
41. Kabantsev, O.V. Deformation properties of masonry as a piecewise homogeneous medium for elastoplastic strain. Earthquake engineering. Constructions safety. 2013. 4. Pp. 36–40.
42. Smirnova, O.M., Menendez Pidal, I., Alekseev, A.V., Petrov, D.N., Popov, M.G. Strain Hardening of Polypropylene Microfiber Reinforced Composite Based on Alkali-Activated Slag Matrix. Materials. 2022. 15(4). Article no. 1607. DOI: 10.3390/ma15041607
43. Calderón, S., Sandoval, C., Araya-Letelier, G., Aguilar, V. A detailed experimental mechanical characterization of multi-perforated clay brick masonry. Journal of Building Engineering. 2023. 63(B). Article no. 105505. DOI: 10.1016/j.jobe.2022.105505
44. Donnini, J., Maracchini, G., Lenci, S., Corinaldesi, V., Quagliarini, E. TRM reinforced tuff and fired clay brick masonry: Experimental and analytical investigation on their in-plane and out-of-plane behavior. Construction and Building Materials. 2021. 272. Article no. 121643. DOI: 10.1016/j.conbuildmat.2020.121643
45. Laskov, N.N., Laskov, A.N., Artucshin, D.V. The influence of the thickness brick sewer on toughness under joint action vertical and horizontal power. Ėffektivnye stroitel'nye konstruktsii: teoriia i praktika [Efficient building structures: theory and practice]. 2019. Pp. 78–82.
46. Derkach, V.N. Tangential adhesion strength of cement mortars in masonry. Magazine of Civil Engineering. 2012. 29(3). Pp. 19–28. DOI: 10.5862/MCE.29.2
47. Demchuk, I.E., Derkach, V.N. Research of the bonding strength of mortar in masonry. Vestnik of Brest State Technical University. 2012. 1(73). Pp. 70–75.
48. Derkach, V.N. Normal cohesive strength of cement mortar in the masonry. Magazine of Civil Engineering. 2012. 33(7). Pp. 6–13. DOI: 10.5862/MCE.33.1
49. Üçer Erduran, D., Elias-Ozkan, S.T., Ulybin, A. Assessing potential environmental impact and construction cost of reclaimed masonry walls. International Journal of Life Cycle Assessment. 2020. 25(2). Pp. 1–16. DOI: 10.1007/s11367-019-01662-2
50. Pelà, L., Canella, E., Aprile, A., Roca, P. Compression test of masonry core samples extracted from existing brickwork. Construction and Building Materials. 2016. 119. Pp. 230–240. DOI: 10.1016/j.conbuildmat.2016.05.057
51. Pelà, L., Kasioumi, K., Roca, P. Experimental evaluation of the shear strength of aerial lime mortar brickwork by standard tests on triplets and non-standard tests on core samples. Engineering Structures. 2017. 136. Pp. 441–453. DOI: 10.1016/j.engstruct.2017.01.028
52. Ghimire, A., Noor-E-Khuda, S., Ullah, S.N. et al. Determination of Mohr–Coulomb failure envelope, mechanical properties and UPV of commercial cement-lime mortar. Materials and Structures. 2022. 55(4). Pp. 1–19. DOI: 10.1617/s11527-022-01959-z
53. Hayen, R., Schueremans, L., Van Balen, K., Van Gemert, D. Triaxial testing of historic masonry, test set-up and first results. WIT Transactions on the Built Environment. 2001. 55. Pp. 151–160.
54. Hayen, R., Van Balen, K., Van Gemert, D. Triaxial interaction of natural stone, brick and mortar in masonry constructions. Building Materials and Building Technology to Preserve the Built Heritage. 2009. Pp. 333–352.
55. 55. Onishchik, L.I. Kamennye konstrukcii [Stone constructions]. Moscow: Strojizdat, 1939. 412 p.
56. Onishchik, L.I. Prochnost' i ustojchivost' kamennyh konstrukcij [Strength and stability of stone structures]. Moscow: ONTI, 1937. 276 p.
57. de Felice, G., Amorosi, A., Malena, M. Elasto-plastic analysis of block structures through a homogenization method. International Journal for Numerical and Analytical Methods in Geomechanics. 2010. 34(3). Pp. 221–247. DOI: 10.1002/nag.799
58. Heyman, J. The stone skeleton. International Journal of Solids and Structures. 1966. 2(2). Pp. 249–279. DOI: 10.1016/0020-7683(66)90018-7
59. Ofrikhter, I.V., Ponomaryov, A.B., Zakharov, A.V., Shenkman, R.I. Estimation of soil properties by an artificial neural network. Magazine of Civil Engineering. 2022. 110(2). Article No. 11011. DOI: 10.34910/MCE.110.11

60. Verbilo, P.E., Vilner, M.A. Study of the jointed rock mass uniaxial compression strength anisotropy and scale effect. MIAB – Mining Informational and Analytical Bulletin. 2022. 6−2. Pp. 47–59. DOI: 10.25018/0236_1493_2022_62_0_47
61. Ulybin, A.V., Zubkov, S.V. Control methods for strength of ceramic bricks in the inspection of buildings. Magazine of Civil Engineering. 2012. 3(29). Pp. 29–34. DOI: 10.5862/MCE.29.3
62. Belentsov, Yu.A., Kharitonov, A.M., Leykin, A.P. Evaluation of the bearing capacity of the historical buildings' masonry. Bulletin of civil engineers. 2021. 4(87). Pp. 79–85. DOI: 10.23968/1999-5571-2021-18-4-79-85
63. Vermeer P.A., De Borst, R. Non-associated plasticity for soils, concrete and rock. Heron. 1984. 29(3). Pp. 5–64.
64. Pepe, M., Sangirardi, M., Reccia, E., Pingaro, M., Trovalusci, P., de Felice, G. Discrete and Continuous Approaches for the Failure Analysis of Masonry. Frontiers in Built Environment. 2020. 6. Article no. 43. DOI: 10.3389/fbuil.2020.00043

Information about the authors:

Gregorii Iovlev, *PhD of Technical Sciences*
ORCID: https://orcid.org/0000-0002-8615-390X
E-mail: gregoriiovlev@gmail.com

Nikita Belov
E-mail: nikita_belov23@mail.ru

Aleksandr Zileev, *PhD of Technical Sciences*
ORCID: https://orcid.org/0000-0001-9586-8379
E-mail: Zileev_AG@pers.spmi.ru

Received: 28.03.2023. Approved after reviewing: 05.06.2024. Accepted: 06.06.2024.